Appl. Phys. B 65, 535–539 (1997)

Applied Physics B Lasers and Optics

Reflection holograms in iron-doped lithium niobate

S. Riehemann[1], **G. von Bally**[1], **B.I. Sturman**[2], **S.G. Odoulov**[3]

[1] Laboratory of Biophysics, Institute of Experimental Audiology, University of Münster, Robert-Koch-Str. 45, D-48129 Münster, Germany
(Fax: + 49-251/83-5 85 36, E-mail: striehem@gabor.uni-muenster.de)
[2] Institute of Automation and Electrometry, Russian Academy of Sciences, 1 University Ave., 630 090 Novosibirsk, Russia
(Fax: + 17-3832/35 48 51)
[3] Institute of Physics, National Academy of Sciences, 46 Science Ave., 252 650 Kiev 22, Ukraine
(Fax: +380-44/265 15 89)

Received: 7 November 1996/Revised version: 16 December 1996

Abstract. An analysis of different geometries for the recording of reflection gratings in photorefractive crystals of 3 m pointgroup with photovoltaic charge transport is presented. Several unusual optical geometries are proposed and analyzed in contrast to the traditional arrangement with two counterpropagating ordinary waves recording a grating in a Z-cut sample. Some of these schemes involve the recording of gratings by two eigenwaves with different polarizations and reconstruction of the object wave with orthogonal polarization with respect to the reference wave; this allows noise reduction in holographic reconstruction by simple polarization filtering.

PACS: 42.40.Pa; 72.40.+w; 42.65.Hw

Nowadays there is a certain renaissance in the interest of researchers in recording reflection holographic gratings. The reasons are diverse but nearly always connected to possible applications of this type of holograms. Reflection gratings in photorefractive crystals are attractive for many reasons, e.g., for the design of permanent optical memory with high capacity [1] and their use in solving the problem of a phase conjugator with wide acceptance angle [2]. Recently they were used to develop narrow-band spectral filters [3]. High-resolution imaging with Denisyuk type holograms in photorefractive materials [4] is also an important implementation of reflection gratings. Some interesting new physical phenomena like hexagon pattern formation also involve reflection hologram recording [5–7].

The possibility of recording reflection holograms in photorefractive iron-doped $LiNbO_3$ is known for quite a long time [8], inspite of the fact that most frequently this material is used for transmission hologram recording. Usually two nearly counterpropagating ordinary waves record the reflection grating in a sample with the optical axis perpendicular to its input/output surfaces (Z-cut sample). This kind of recording has been used to get coherent oscillation with four-wave mixing in linear cavity [9] or to develop a selfstarting nonlinear mirror for a Cu-vapor laser [10].

The purpose of this paper is to show that several other possibilities exist to record reflection gratings in crystals with photovoltaic charge transport like lithium niobate.

1 Recording and readout processes in doped $LiNbO_3$

The main charge transport process in iron-doped $LiNbO_3$ is the bulk photovoltaic effect [11, 12]. When a short–circuited crystal is continuously illuminated the steady-state current $\boldsymbol{j}$ appears which is related to the electric field $\boldsymbol{E}$ of the light wave via the third-rank photovoltaic tensor [12]:

$$j_i = \beta_{ijk} \boldsymbol{E}_j \boldsymbol{E}_k^* \,. \tag{1}$$

For $3m$ point group crystals like $LiNbO_3$ the real part of the photovoltaic tensor (symmetric in the last two indices) has four independent components: $\beta_{333},\ \beta_{311} \equiv \beta_{322},\ \beta_{222} \equiv \beta_{211} \equiv \beta_{121},\ \beta^{\mathrm{s}}_{131} \equiv \beta^{\mathrm{s}}_{113}$, and the imaginary part (antisymmetric in the last two indices) has one independent component, $\beta^{\mathrm{a}}_{131} \equiv \beta^{\mathrm{a}}_{113} (\beta_{131} = \beta^{\mathrm{s}}_{131} + \mathrm{i}\beta^{\mathrm{a}}_{131})$. We will use in the following the contracted indices according to the usual convention: $33 \to 3,\ 22 \to 2,\ 11 \to 1,\ 21 \to 6,\ 31 \to 5,\ 32 \to 4$.

When two coherent light waves with a total electric field of

$$\boldsymbol{E} = \boldsymbol{e}_1 A_1 \exp(\mathrm{i}\boldsymbol{k}_1 \boldsymbol{r}) + \boldsymbol{e}_2 A_2 \exp(\mathrm{i}\boldsymbol{k}_2 \boldsymbol{r}) \tag{2}$$

($\boldsymbol{e}_{\mathrm{i}}$ stands for the polarization unit vector, A_1 for the complex amplitude of the light wave, and $\boldsymbol{k}_{\mathrm{i}}$ for the wavevector of each wave) are propagating inside the sample, they produce fringes of light intensity (for identically polarized waves, i.e. $\boldsymbol{e}_1 \cdot \boldsymbol{e}_2 = 1$) or polarization fringes (for orthogonally polarized recording waves, $\boldsymbol{e}_1 \cdot \boldsymbol{e}_2 = 0$).

This spatial modulation of light intensity or light polarization results in the excitation of a spatially modulated photovoltaic current $\boldsymbol{j}(\mathrm{r})$ and leads to the formation of a space-charge grating with the grating vector $\boldsymbol{K} = \boldsymbol{k}_1 - \boldsymbol{k}_2$. The steady-state electric space charge field of

$$\boldsymbol{E}_{\mathrm{sc}}(r) = \boldsymbol{j}(r)/\sigma \,, \tag{3}$$

modulates the optical dielectric tensor $\hat{\varepsilon}$ of the crystal via the linear electrooptic effect:

$$\Delta\hat{\varepsilon}_{lm}^{-1} \propto r_{lmn} E_n^{sc} . \quad (4)$$

So a volume phase grating appears. Here r_{lmn} is the third rank tensor of the linear electrooptic effect and σ is the crystal conductivity.

Each of the two recording waves can be diffracted from the recorded grating. The diffracted part of the first recording beam has the same wavevector $\boldsymbol{k}$ and the same polarization vector $\boldsymbol{e}$ as the second recording beam (and vice versa). The readout of the grating is possible for any geometry where gratings can be recorded, because the structure of the electrooptic tensor is similar to the structure of the photovoltaic tensor. Any nonvanishing component of the electrooptic tensor always corresponds to a certain nonvanishing component of the photovoltaic tensor (with the same indices but in different order, e.g. β_{31} and r_{13})[1]. This is why we always find a readout process (involving the appropriate component of the electrooptic tensor $\hat{r}$) to each particular process of recording (involving a component of the photovoltaic tensor $\hat{\beta}$). So, in the next paragraph, we consider the different possibilities for recording reflection gratings in crystals with the bulk photovoltaic effect.

2 Reflection holograms in crystals with the bulk photovoltaic effect

The simplest (but not always the most advantageous) situation occurs when the sample is cut along its crystallographic directions, i.e., its faces are normal to X, Y, and Z directions, and the writing waves are incident upon the sample normal to its faces ($\boldsymbol{k}_1 = -\boldsymbol{k}_2$). It is quite clear that in this case we can write either gratings with $\boldsymbol{K}||\boldsymbol{OZ}$ with the currents related to β_{31} and β_{32} components of the photovoltaic tensor or gratings with $\boldsymbol{K}||\boldsymbol{OY}$ with the current related to β_{21}. These two allowed geometries are shown in Figs. 1a and 1b. Because the light waves are transvers waves (their electric displacement vector $\boldsymbol{D}$ is normal to their wavevector $\boldsymbol{k}$) we cannot exploit β_{33} (or β_{22}) to record a grating with $\boldsymbol{K}||\boldsymbol{OZ}$ (or $\boldsymbol{K}||\boldsymbol{OY}$). It is also not possible to use β_{16} to record a grating with $\boldsymbol{K}||\boldsymbol{OX}$.

For unusual cuts of the sample, when the grating vector $\boldsymbol{K}$ is not directed along one of the crystallographic axes, all components of the photovoltaic tensor can be used to record reflection gratings.

Let us consider, for example, the orientation shown in Fig. 1c. Here the optical axis of the crystal is tilted 45 ° to the normal of the sample input face, but the light waves are still incident normal to the sample faces. The two writing waves are now extraordinary waves and the polarization vectors $\boldsymbol{e}_{1,2}$ have both Z-components and X-(or Y-) components. It means that besides the current related to the component β_{31} we have now also the current related to β_{33}.There is no current along the X-axis related to $\beta_{11} \equiv 0$ or $\beta_{13} \equiv 0$, but the current related to β_{15} also exists. For (011)-cut one extra current, related to β_{22} , also contributes to the space-charge formation.

[1]The only difference is that the electrooptic tensor has no imaginary components corresponding to β_{15}^{a}. Fortunately it has the real component with the same indices r_{51}; this ensures the diffraction from the grating recorded by currents related to β_{15}^{a} as well as to β_{15}^{s}.

The other possibility is to use orthogonally polarized waves to record reflection holograms in a crystal with a (101) input face (Fig. 1d). Here the charge separation is based on the excitation of a photovoltaic current related to the β_{16} component. It is seen that none of the other components are involved in grating recording in this geometry (neither producing a current along $\boldsymbol{OX}$ nor along $\boldsymbol{OZ}$).

In samples with the (011) input face and with incident waves polarized as shown in Fig. 1e two other components, related to β_{21} and β_{31}, are contributing to the reflection grating recording.

And finally, for samples with a (110) input face, two components of current, related to β_{22} and β_{16}, are active in reflection grating formation (Fig. 1f).

The diffraction efficiency in the limit of a small grating strength is proportional to the light-induced change of the electric (high-frequency) permittivity (see, e.g., [13])

$$\eta \propto (\Delta n)^2 \propto \Delta\varepsilon , \quad (5)$$

which, in turn, is proportional to the product of the effective electrooptic and photovoltaic coefficients for any particular orientation of the crystal axes [(1) to (4)]

$$\Delta\varepsilon \propto (r_{\text{eff}}\beta_{\text{eff}}) . \quad (6)$$

Thus we can consider the product $(r_{\text{eff}}\beta_{\text{eff}})$ as a figure of merit for the grating efficiency.

To calculate the effective electrooptic and photovoltaic coefficients for particular crystal cuts one can use the general

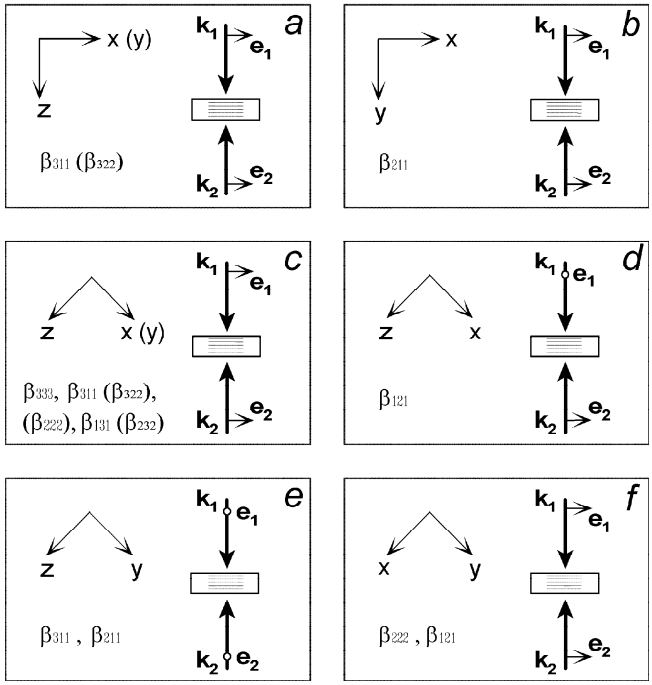

Fig. 1. Possible optical configurations for recording of reflection holograms (see text). Orientation of the crystallographic axes is shown on the left side of every box while orientation of the incident waves and their polarizations are shown on the right side. In the lower left-hand corner the photovoltaic constants are shown which assure the charge transport for this particular configuration

expressions

$$r_{\text{eff}} = r_{kmn} e_k^{\gamma} e_m^{\delta} \nu_n \ , \tag{7}$$

and

$$\beta_{\text{eff}} = \beta_{ijl} \nu_i e_j^{\alpha} e_l^{\beta} \ , \tag{8}$$

where e_p^{ζ} are the components of the polarization unit vectors for the two recording waves, superscripts $\zeta = 1$ and 2 denote the waves 1 and 2, respectively; subscripts $p = 1, 2$, and 3 correspond to the Cartesian components of the $\boldsymbol{OX}$, $\boldsymbol{OY}$, and $\boldsymbol{OZ}$ axes, and ν_q are the Cartesian components of the grating unit vector, $\boldsymbol{\nu} = \boldsymbol{K}/K$.

We present below the expressions for r_{eff} and β_{eff} for the orientations shown in Figs. 1a to 1f. For samples cut along the crystallographic axes these expressions take the simplest form

$$(\mathbf{a}) \quad r_{\text{eff}} = r_{13} \ , \qquad \beta_{\text{eff}} = \beta_{31} \ , \tag{9}$$

$$(\mathbf{b}) \quad r_{\text{eff}} = -r_{22} \ , \qquad \beta_{\text{eff}} = -\beta_{22} \ . \tag{10}$$

For different geometries with 45°-cut crystals the effective coefficients are

$$(\mathbf{c}) \quad r_{\text{eff}} = (1/\sqrt{8})(r_{33} + r_{13} - 2r_{51}) \ , \tag{11}$$
$$\beta_{\text{eff}} = (1/\sqrt{8})(\beta_{33} + \beta_{31} - 2\beta_{15}^{\text{s}}) \ ,$$

$$(\mathbf{d}) \quad r_{\text{eff}} = -(1/2) r_{22} \ , \qquad \beta_{\text{eff}} = -(1/2)\beta_{22} \ , \tag{12}$$

$$(\mathbf{e}) \quad r_{\text{eff}} = (1/\sqrt{2}) r_{13} \ , \qquad \beta_{\text{eff}} = (1/\sqrt{2})\beta_{31} \ , \tag{13}$$

$$(\mathbf{f}) \quad r_{\text{eff}} = (1/\sqrt{2}) r_{22} \ , \qquad \beta_{\text{eff}} = (1/\sqrt{2})\beta_{22} \ . \tag{14}$$

In the expressions listed above only the strongest nonvanishing components are kept; r_{22} and β_{22} are omitted in all cases when larger components like r_{33}, r_{13}, r_{51} (β_{33}, β_{31}, β_{15}^{s}) are present (see Table 1) [2].

Note that there is no contribution of the circular photovoltaic current [12] (from the antisymmetric component β^{a} of the photovoltaic tensor) in any considered reflection geometry. This is the consequence of the orthogonality of the grating vector and the polarization vector of the recording wave, $(\boldsymbol{\nu} \cdot \boldsymbol{e} = 0)$.

In Table 1 we summarize the known data on electrooptic and photovoltaic properties of lithium niobate [14–17]. The electrooptic coefficients characterize the crystal host itself and are independent (in first approximation) on the dopant content [14]. The photovoltaic coefficients are on the contrary strongly dependent on the type and amount of impurity in the sample. For doped $LiNbO_3$ with an iron content up to $10^{25}\,\text{m}^{-3}$ the components of the photovoltaic tensor are linearly increasing with the concentration of divalent iron [15, 16]. Therefore the ratios of different components remain the same for any arbitrary doping level. These ratios are also weakly dependent on the wavelength in the blue-green region of spectrum [17, 18]. For this reason we present in addition to the absolute values of β (measured at $\lambda = 470\,\text{nm}$ for $LiNbO_3$ with $4 \times 10^{24}\,\text{m}^{-3}$ of divalent iron) in the third column of Table 1 the values of β normalized to β_{22}, including those for the nondiagonal components β_{15}^{s} and $|\beta_{15}|$.

Table 1. Electrooptic coefficients, absolute and normalized photovoltaic coefficients (see text) of iron-doped $LiNbO_3$ crystals

electrooptic coefficients pm/V [14]	photovoltaic coefficients 10^{-9} A/W [15]	normalized photovoltaic coefficients $\beta_{\text{ij}}/\beta_{22}$
$r_{33} = 32.0$	$\beta_{33} = 52.0$	$\beta_{33}/\beta_{22} = 11.6$
$r_{13} = 7.7$	$\beta_{31} = 62.5$	$\beta_{31}/\beta_{22} = 13.9$
$r_{22} = 3.4$	$\beta_{22} = 4.5$	$\beta_{22}/\beta_{22} = 1$
$r_{51} = 28.8$		$\lvert\beta_{15}\rvert/\beta_{22} = 4.0$ [16]
		$\beta_{15}^{\text{s}}/\beta_{22} < 0.4$ [16]

These data allow the evaluation of the ratios of figures of merit ($r_{\text{eff}}\beta_{\text{eff}}$) for any of the considered optical arrangements of reflection grating recording, and therefore to compare their relative diffraction efficiencies.

3 Experiment

The aims of our measurements are to check the efficiency of recording holographic gratings in several proposed geometries and to study the possibility of polarization filtering of scattering noise from the readout wave in case of geometry (**d**) (see Fig. 1).

The iron-doped lithium niobate crystals used in the experiments contain approximately 0.02 to 0.03 wt.% of iron in the melt. Two samples are used, one with all faces polished, measuring 6.01 mm × 6.98 mm × 4.86 mm along X, Y, and Z directions, respectively. The second sample has only two pairs of faces polished, one normal to the [010]-direction (thickness 3.56 mm) and the other normal to the [101]-direction (thickness 3.49 mm). The samples are cut from different ingots of unknown origin, sample 2 has a slightly deeper color compared with sample 1.

A single-mode, single-frequency Ar^+-laser ($\lambda = 514.5\,\text{nm}$) is used for hologram recording. The laser beam is expanded to 10 mm in diameter to assure uniform illumination of the sample. The total intensity of the recording beams is about $160\,\text{mW/cm}^2$ and the contrast of the recording fringes is $m = 0.97$. One of the two beams is directed to the sample normally to the input face while the other is tilted about $\alpha = 17°$ to the face normal (so the diffracted and transmitted beam can be detected directly, without using a beam-splitter and thus without loosing intensity).

For several geometries listed in Fig. 1 the dynamics of diffracted light intensity is studied during grating recording and optical erasure. The temporal development of the grating efficiency is relatively seldomly smooth and regular. The typical time behaviour is shown in Fig. 2 for geometry (**e**) (see Fig. 1), sample 2. For other geometries the dynamics were similar. Most often the growth of intensity is frequently interrupted by a sudden fall in the efficiency and a subsequent rather fast increase. The reason for these irregular kinetics is known quite well for doped lithium niobate crystals: it is related to the accumulation of a high large-scale space charge field and subsequently repeating breakdowns. In these conditions only a qualitative comparison of the experimental

[2] One can include these smaller contributions by using the following relationship for a correction factor to r_{eff} : $\delta r_{\text{eff}} = r_{22}[\nu_2(e_2^1 e_2^2 - e_1^1 e_1^2) - \nu_1(e_1^1 e_2^2 + e_2^1 e_1^2)]$.

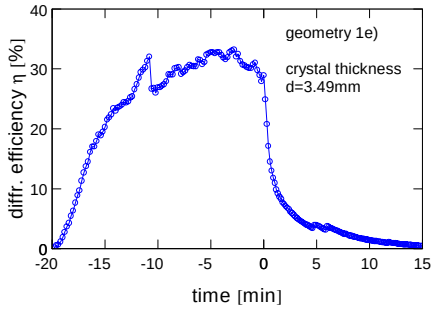

Fig. 2. Dynamics of the diffraction efficiency during hologram recording and optical erasure for sample 2, geometry of Fig. 1e. Here the recording is stopped after $t = 20$ min

findings with calculations can be performed. We believe the ratios of the measured diffraction efficiencies for different geometries are less affected by these factors than the diffraction efficiencies themselves.

Table 2 shows the largest values of diffraction efficiency measured for different geometries of the reflection hologram recording. As the exact content of iron is unknown for our samples it is only possible to compare results received with the same crystal. For sample 1 the diffraction efficiency for geometry (**a**) is larger than for geometry (**b**) in spite of the fact that the hologram thickness is smaller for case (**a**). This is in qualitative agreement with our expectations, as $\beta_{22}r_{22} < \beta_{31}r_{13}$. For sample 2 the measured values are also in agreement with our expectations. The largest efficiency corresponds to geometry (**e**) where the strongest photovoltaic current related to β_{31} is involved in space charge formation; the smallest efficiency corresponds to geometry (**d**) where the weakest current related to β_{22} is responsible for grating recording. Note that even in this case the efficiency is in the order of 4×10^{-3} which is sufficient for many applications. At the same time the advantage of this geometry compared with others is the orthogonal polarization of the reconstructed image wave compared with the polarization of the incident readout wave. This raises the possibility of cutting all scattered light with the same polarization as the readout wave by utilizing a polarizer adjusted to transmit the reconstructed wave only.

With geometry (**d**) a reflection hologram of a standard transparent resolution chart is recorded in sample 2. For this puspose the 514.5 nm output of an Ar^+-laser with a total intensity of 120 mW/cm^2 is used. The contrast of the recording fringes is about $m = 0.9$, the exposure time during the recording is 5 s. The transparent resolution chart is placed

Table 2. Recording geometry, used sample, sample thickness, and diffraction efficiency of reflection holograms recorded in iron doped $LiNbO_3$ crystals

geometry (Fig. 1)	sample	thickness d/mm	diffraction efficiency η
(**a**)	1	4.86	0.11
(**b**)	1	6.98	0.10
(**c**)	2	3.49	0.08
(**d**)	2	3.49	0.004
(**e**)	2	3.49	0.33

Fig. 3. Image of a resolution chart reconstructed from a reflection hologram recorded in geometry of Fig. 1d, sample 2

in the object beam during recording. An image of the reconstructed hologram is recorded digitally with the help of a CCD-camera. The readout time is 20 ms. Figure 3 represents the reconstructed image of the test chart. This image is simply an example of a typical hologram recording, and does not show the maximum achievable resolution. The ultimate resolution in the image plane can be evaluated from the angular dependence of the diffraction efficiency as shown in Fig. 4. This dependence is measured with a plane image wave coming to the sample at different tilt angles in a plane containing the [100] and [001] axes of the sample while the direction of the reference wave is kept constant. Evaluating in such a way an acceptance angle of $\pm 30°$ in air ($\pm 12°$ in crystal) for the image spatial spectrum, we come to conclusion that even with this reduced acceptance angle, images with submicron resolution can be stored. This has already been demonstrated for reflection hologram recording with another photorefractive crystal, cerium-doped strontium barium niobate [4].

The angular dependence of diffraction efficiency, as plotted in Fig. 4, cannot be explained by taking into account only the angular dependence of material parameters (electrooptic

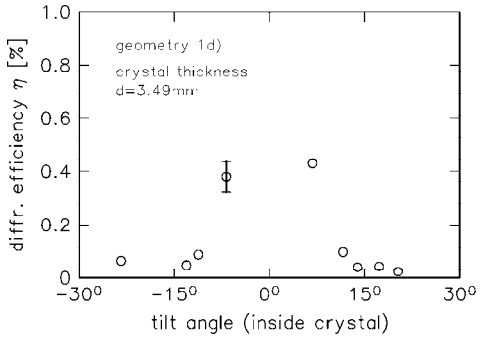

Fig. 4. Diffraction efficiency of gratings recorded in sample 2 in geometry of Fig. 1d as a function of the tilt angle (inside the sample) of a plane object wave. The misalignment of this beam is in the crystallographic (101) plane

and photovoltaic coefficients), changing the tilt angle of grating vector, or changing the light intensity inside the sample and so changing photovoltaic fields. It may be that the strong reduction of diffraction efficiency for large illumination angles is based on shadowed areas inside the sample and so on nonuniform space charge fields (see e.g. [19]).

4 Conclusions

Several proposed arrangements for reflection grating recording in iron-doped $LiNbO_3$ crystals were analyzed and studied experimentally. All of them assure a diffraction efficiency of the recorded grating on the order of 10^{-1} to 10^{-3} in a few mm thick sample, which is sufficient for practical applications such as image recording, holographic interferometry, etc.

One of the proposed reflection hologram orientations assure recording by orthogonally polarized light waves and permit polarization filtering of the reconstructed image to reduce scattered light. At the same time the theoretically possible diffraction efficiency of gratings in all proposed reflection-type configurations is smaller than in the classical Z-cut arrangement shown in Fig. 1a. This configuration remains unique as it assures the largest (and axially symmetric) acceptance window for spatial frequencies of the recorded object wave.

Acknowledgements. The authors want to thank F. Rickermann for helpful discussions and the reviewer for valuable suggestions. Financial support of the Deutsche Forschungsgemeinschaft (SFB 225/D7) is gratefully acknowledged.

References

1. G.A. Rakuljic, V. Leyva, A. Yariv: Opt. Lett. **17**, 1471 (1992)
2. T. Honda, H. Matsumoto: J. Opt. Soc. Am. B **11**, 1983 (1994)
3. G.A. Rakuljic, V. Leyva: Opt. Lett. **18**, 459 (1993)
4. G. von Bally, S. Riehemann, F. Rickermann: Opt. Commun. **133**, 305 (1996)
5. T. Honda: Opt. Lett. **18**, 598 (1993)
6. T. Honda: Opt. Lett. **20**, 851 (1995)
7. T. Honda, H. Matsumoto: Opt. Lett. **20**, 1755 (1995)
8. P. Günter, J.P. Huignard (Eds.): *Photorefractive Materials and Their Applications I*, Topics in Applied Physics Vol. **61** (Springer, Berlin, Heidelberg 1988) pp.7–70
9. S. Odoulov, M. Soskin: Sov. Phys. JETP Lett. **37**, 298 (1983)
10. A. Litvinenko, S. Odoulov: Opt. Lett. **9**, 68 (1984)
11. A.M. Glass, D. von der Linde, T. Negran: Appl. Phys. Lett. **25**, 233 (1974)
12. V. Belinicher, B. Sturman: Sov. Phys. Uspekhy **23**, 199 (1980)
13. M.P. Petrov, S.I. Stepanov, A.V. Khomenko: *Photorefractive Crystals in Coherent Optical Systems*, Series in Optical Sciences Vol. **59** (Springer, Berlin, Heidelberg 1991)
14. S.H. Wemple, M. Di Domenico, I. Camlibel: J. Phys. Chem. Solids **29**, 1797 (1968)
15. H.G. Festl, P. Hertel, E. Krätzig, R. von Baltz: phys. stat. solidi (b) **113**, 157 (1982)
16. S. Odoulov: Ferroelectrics **91**, 213 (1988)
17. S. Karabekian: Sov. Solid State Phys. **33**, 633 (1991) (in russian)
18. S. Karabekian, S. Odoulov: phys. stat. solidi (b) **169**, 529 (1992)
19. D.M. Shields, T.E. Luke: Opt. Commun. **55**, 391 (1985)